25^{th} Computer Vision Winter Workshop
Domen Tabernik, Alan Lukei, Klemen Grm (eds.)
Rogaka Slatina, Slovenia, February 3–5, 2019

Practical high-speed motion sensing: event cameras vs. global shutter

Ondřej Holešovský, Václav Hlaváč, Radoslav Škoviera
Czech Technical University in Prague
Czech Institute of Informatics, Robotics, and Cybernetics
160 00 Praha 6, Dejvice, Jugoslavských partyzánů 1580/3, Czech Republic
ondrej.holesovsky@cvut.cz https://people.ciirc.cvut.cz/holesond/

Roman Vítek
University of Defence in Brno
Faculty of Military Technology, Department of Weapons and Ammunition
662 10 Brno, Kounicova 65, Czech Republic
roman.vitek@unob.cz

Abstract. *We designed two maximally simplified and controlled experiments to test event-based and frame-based cameras in the price category affordable for an ordinary university research lab. First, we put common ArUco markers on a rotating disk and observed them by both types of cameras. We reconstructed the image from an event camera using a publicly available state-of-the-art algorithm and compared the ArUco marker recognition reliability. Surprisingly, our results suggest that the ability of the tested event camera to recognise quickly moving markers is inferior to an affordable* 1000 *fps frame-based camera. In the second experiment, we let the cameras observe a freely flying subsonic pistol projectile. A very expensive* 20000+ *fps camera provided ground-truth images, as the acquisition rate of the affordable frame-based camera was insufficient. Although event camera data was partially corrupt, it still allowed us to estimate the position of the small projectile every* 10 μ*s, when the projectile translated mostly along the event camera pixel rows.*

1. Introduction

Independent pixels of event cameras [1] generate asynchronous events in response to local log intensity changes. Each pixel performs a level-crossing sampling of the difference of logarithmic brightness sensed by the pixel. Each time the difference passes a preset threshold, the pixel emits a change detection (CD) event and resets its brightness reference to the current brightness. A CD event is characterised by its pixel coordinates, its precise timestamp in microsecond resolution, and the polarity of the brightness change. The advantages of event cameras over traditional cameras include lower sensor latency, higher temporal resolution, higher dynamic range (120 dB+ vs. 60 dB of traditional cameras), implicit data compression, and lower power consumption.

This work gives a partial answer to the fundamental question of applicability of event cameras: What are the applications, in which event cameras cannot be replaced by high-speed cameras capturing sequences of image frames? The answer to this question, however, is not so straightforward. Our initial hypothesis was that the superiority of event cameras comes from the fast capture of asynchronous events only from pixels where changes happen, as compared to the full frame readout in ordinary frame-based cameras. This phenomenon should be even stronger when changes in the scene are rather local.

Initially, we tested the limits of our ATIS event camera at a partner university in a very fast experiment when observing a flying bullet. Surprisingly, the motion speeds and scene complexities the event camera could record well were lower than we expected. Moreover, we observed strange phenomena in the event recordings.

In general, the speed limits of event cameras depend on two factors:

1. The pixel bandwidth and sensitivity restricts which light changes can be detected by a pixel.

2. The ability of the digital sensor logic to read out events from the pixel array correctly and in time restricts the spatial and temporal distribution of events in the pixel array.

We tested these limits in two experimental settings, namely on the detection of quickly rotating ArUco markers and on the position tracking of a flying projectile fired from a firearm. We compare event camera results to images captured by high-speed global shutter cameras.

2. Related work

There is a recent survey by Gallego et al. [2] mentioning several different event camera application areas. The mentioned areas are real-time interaction systems, object tracking, surveillance, object recognition, depth estimation, optical flow, 3D structured light scanning, high dynamic range (HDR) imaging, video compression, visual odometry, and image deblurring.

Event cameras attract growing attention, which was demonstrated at the Second International Workshop on Event-based Vision and Smart Cameras at CVPR in June 2019 [3].

To the best of our knowledge, however, the literature dealing with head-to-head comparisons of event and common frame-based cameras is quite limited.

A common (frame-based) monochrome camera provides as its output the sequence of grayscale images naturally. Reconstruction of images from an event camera is more complicated. The state-of-the-art approach to cope with this task was published in Rebecq et al. [4]. Among other things, the authors compare the quality of images reconstructed from events to standard camera frames. The reconstructed images better capture the dynamic range of the scene than the standard frames. The authors also compare visual-inertial odometry algorithms running on traditional camera frames and on images reconstructed from events. Event-based reconstructed intensity image results are reported to be on average superior not only to the results of traditional frames, but also to the state-of-the-art methods running on events directly. However, the first is no surprise as the chosen traditional camera frame rate was only 20 frames per second and the captured frames suffered from severe motion blur likely due to the too long exposure time.

Falanga et al. [5] analyse the response latency of obstacle avoidance of a quadrotor drone with a mounted camera. The obstacle size and shape was assumed to be known. Their event-based algorithm was able to detect the obstacle whenever a displacement of at least five pixels occurred. Given drones available at that time, the authors concluded that an event camera with resolution 320×262 pixels gave obstacle detection latencies comparable to standard stereo cameras running at 60 fps. Increasing the resolution of event cameras might make them a better solution, as the ability to sense a distant obstacle depends on sufficiently high spatial sensor resolution. However, most of the analysis was done theoretically. Experiments were only done with the event camera, not with the standard cameras.

Barrios-Avilés et al. [6], probably the closest work to ours, also test the object detection latency of event and standard cameras. Their vision system detects a black circular dot rotating on a white disk and estimates the position of the dot for control purposes. Surprisingly, the authors report latency differences between the two cameras in the order of 100 ms, despite the frame rate of the standard camera being 64 fps at VGA image resolution. It is unlikely that such long latency would be caused by the cameras or by the object detection algorithm based on image intensity thresholding running on the standard camera frames.

3. Method

We test the speed limits of an event camera on the task of reading ArUco markers [7] in motion. The name ArUco originates in a free software library [1] for processing the markers. The markers placed on a disk are rotated at a gradually increasing velocity, which is measured independently by a rotary encoder, see Figure 1.

Raw CD events on their own do not suffice for the detection of typical markers. To alleviate this problem, we utilise a state-of-the-art method for intensity image reconstruction from events. One such method, E2VID[2] was presented in [8] and [4].

The intensity image reconstruction method E2VID [4] utilises a recurrent convolutional neural network whose architecture is similar to UNet. In each iteration, the network computes a reconstructed intensity image as a function of a batch of events and a sequence of K previously reconstructed intensity images. The authors stored each event batch for the network input into a spatio-temporal voxel grid.

[1] https://www.uco.es/investiga/grupos/ava/node/26

[2] code: https://github.com/uzh-rpg/rpg_e2vid

The network was trained in a supervised mode on simulated event sequences and corresponding ground-truth intensity images.

We measure marker detection performance by two metrics, namely detection count and detection reliability. We define marker detection reliability r as

$$r = \frac{1}{N_r N_m} \sum_{i=0}^{N_r} M_i, \tag{1}$$

where M_i is the number of detected unique marker IDs within revolution i, N_r is the total number of recorded revolutions, N_m is the number of unique marker IDs printed on the disk. Detection count c is

$$c = \frac{1}{N_r N_m} \sum_{j=0}^{N_m} I_j, \tag{2}$$

where I_j is equal to the number of times the marker ID j is detected within N_r revolutions.

4. Implementation

We use the ATIS HVGA Gen3 event camera kit PSEE350EVK (from Prophesee[3]).We experimentally estimated the maximum data bandwidth to be approx. 22 million events per second, by rotating the camera with a telelens as fast as possible while looking at a densely textured scene. We mounted a lens with the focal length of 25 mm. The sensor generates both the standard change detection (CD) events, as well as asynchronous exposure measurement (EM) events. An older generation of the ATIS camera is described in [9]. In this work, we utilise only the simpler CD events, so that results can be applied to other event cameras such as [1] or [10]. The size of the photodiode of the change detector is not stated directly by the manufacturer. However, we expect this area to be at least 10% of the pixel area, which is the CD fill factor reported for the previous sensor generation in [9]. Thus, the size of the photodiode should be at least $20 \cdot 20 \cdot 0.1 = 40\ \mu m^2$. The change detector sensitivity parameter is in the range from 0 (least sensitive) to 100 (most sensitive).

All parameters in the reconstruction method [4] were kept at the defaults, except the number of events used for the reconstruction of a single intensity image. Unless noted otherwise, we set this number to 8640 events per frame, which enables good reconstruction of the markers we are using on plain white background. The effect of changing this parameter is investigated further in the experiments.

camera	ATIS	Photron	Basler
resolution $[px]$	480×360	1024×1024	480×360
pixel size $[\mu m]$	20×20	20×20	4.8×4.8
exposure $[\mu s]$	-	1	59*
frame rate [FPS]	-	20000	1000**

* exposure time in weak lighting conditions was 3000 μs
** 300 FPS was used during weak lighting conditions

Table 1: Camera parameters and experiment conditions

Our chosen fast global shutter camera is the Basler acA640-750um USB 3.0 camera [4]. Basler pixel area is at most 23 μm^2. Therefore, we may assume that the light-sensitive area of the ATIS pixels is at least two times larger than the same area in the Basler pixels.

Additionaly, a high speed camera Photron FastCam SA-Z[5] was used as a reference during tests with the projectiles at the ballistic laboratory of Department of Weapons and Ammunition, University of Defence in Brno. A list of basic parameters for all cameras is listed in Table 1.

ArUco markers were 3×3 mm in size. They were generated from a custom dictionary: 4×4 data squares in each marker, dictionary size 10, random seed 65536. Only marker IDs 1-9 were used. The centres of the nine markers were located on the circumference of the rotating disk, at the radius of 85 mm. A DC motor with controllable rotation speed rotated the disk. A rotary encoder mounted on the motor shaft provided independent angular velocity measurements.

A photo of our experimental setup for comparison of the ATIS and Basler cameras in different lighting conditions is in Figure 1. Both cameras have a similarly-sized field of view, see Figure 2. The Basler camera sees the marker as a square of size 34.1 pixels, the ATIS camera perceives the apparent marker size of 34.4 pixels. We deliberately chose as small markers as possible, in order to maximally reduce the number of events generated by the ATIS sensor per a single pass of a marker across the pixel array. The setup of the balistic experiment with the high-speed camera is shown in Figure 3.

[3] https://www.prophesee.ai/

[4] https://www.baslerweb.com

[5] https://photron.com/fastcam-sa-z/

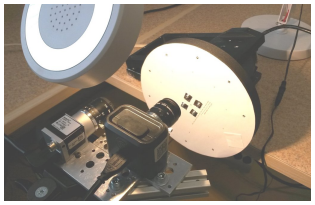

Figure 1: The experimental scene setup with strong lighting. The frame-based Basler (left) and the event-based ATIS (right) cameras are watching the white rotating disk with nine ArUco markers. A nonflickering LED lamp illuminates the scene from the top.

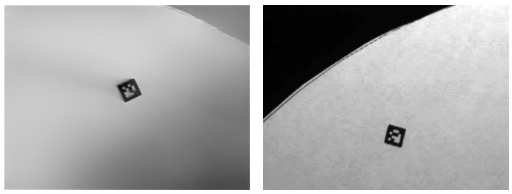

(a) ATIS (b) Basler

Figure 2: The field of view of each camera.

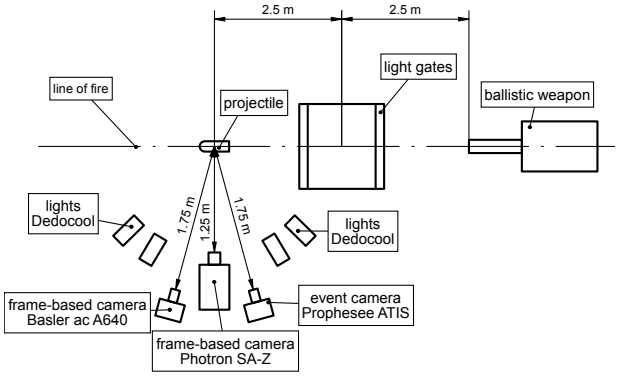

Figure 3: The scene setup of the balistic experiment.

5. Experiments

5.1. Strong lighting

Initially, we used the lamp shown in Figure 1 to strongly illuminate the scene, which is common in industrial settings. With exposure time 59 μs of the Basler camera, the white paper colour has mean intensity values of 61.3 ± 2.5, the black marker colour has mean intensity of 7.0 ± 1.5.

With the Basler camera, ArUco marker detection works reliably up to 25 revolutions per second (rps) or 150 kpx/s image velocity. A 50% detection reliability is reached around 34 rps, see Figure 6. See Figure 7 for sample marker images at different angular speeds.

The images reconstructed from the ATIS events enable reliable marker detection up to 4 rps or 24 kpx/s image velocity with sensitivity set to 40. 50% detection reliability is reached around 6 rps, see Figure 4. With growing rotational speed, the detection reliability of the ATIS decays faster when the sensitivity is set significantly lower or higher than 40, shown in Figure 5. However, the sensitivity value of 60 yields the most detected markers per revolution at low rotational speed, it detects the least markers at higher speeds. See Figure 8 for sample reconstructed marker images at different angular speeds.

Figure 9 shows two batches of recorded events 100 μs long visualised in the image plane. White pixels denote positive, black pixels negative polarity events. At the lower velocity of 3.5 rps, events are mostly read in time from all pixels which generate them. At the higher angular velocity of 6 rps, however, it is more common that no events are read from several pixel rows in the middle of the ArUco marker where events should have been present. Most of the time, the event rate measured in 50 μs intervals of the recording did not exceed 15 Mev/s in the faster case and 12 Mev/s in the slower case.

Reducing the event camera sensitivity setting did not help in raising the speed limits significantly. When the sensitivity is set too low, no events are generated at higher speeds. A sufficiently high sensitivity needs to be set so that the intensity reconstruction algorithm has enough data to reconstruct the intensity well. In the case of 4 rps, for example, lowering the sensitivity from 50 to 20 reduces the highest typical event rate from 15 to 10 million events per second. However, too few events are recorded, see Figure 10 and reliable intensity reconstruction becomes more challenging with very low sensitivity, see Figure 4. Altering the number of events used for the reconstruction of a single image does not help either, see Figure 11. Too few events and fine marker details are easily missed. Too many events and the edges become blurred.

5.2. Weak lighting

Weaker scene lighting is common in more natural or outdoor scenes, where artificial light cannot be conveniently used or is undesirable. We emulate weak lighting at night by a weaker LED lamp with all other light sources turned off, see Figure 12. With weak lighting and exposure time 3000 μs of the Basler camera, the white paper gives mean intensity values of 26.3 ± 4.5, the black marker colour has a

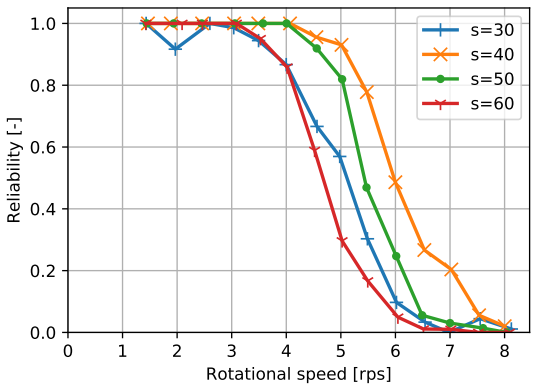

Figure 4: Reliability of marker detection with the ATIS as a function of rotational speed. For several sensitivity settings s. Strong lighting.

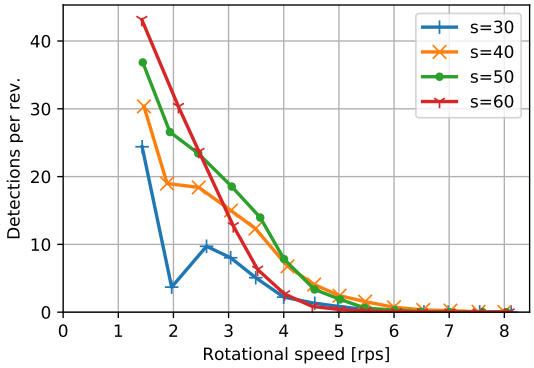

Figure 5: Detection count, i.e. mean number of single marker detections per revolution with the ATIS as a function of rotation speed. For several sensitivity settings s. Strong lighting.

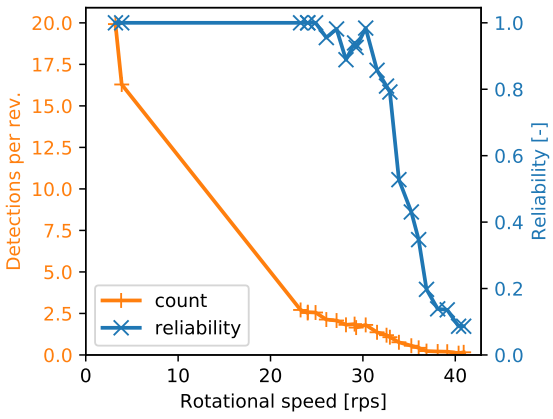

Figure 6: Reliability of marker detection and mean count of single marker detections per revolution as functions of rotational speed. Basler camera, strong lighting.

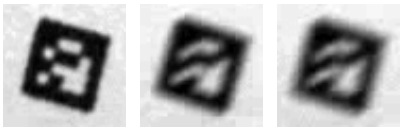

(a) 4.0 rps (b) 23 rps (c) 30 rps

Figure 7: Sample images of an ArUco marker captured by the Basler camera. Strong lighting, exposure time 59 μs. Different rotational speeds.

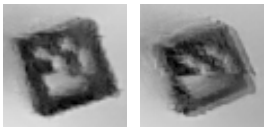

(a) 3.5 rps (b) 6.0 rps

Figure 8: Sample ATIS reconstructions of an ArUco marker from 8640 events per frame. Sensitivity 40, strong lighting.

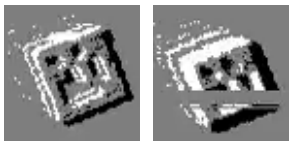

(a) 3.5 rps. (b) 6.0 rps.

Figure 9: 100 μs of recorded ATIS events at different rotational velocities. Sensitivity 40, strong lighting.

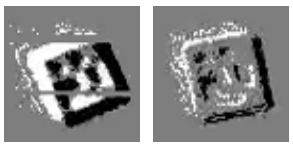

(a) $s = 50$. (b) $s = 20$.

Figure 10: 100 μs of recorded ATIS events at 4 rps using different sensitivities s. Strong lighting.

(a) 2073 ev. (b) 4620 ev. (c) 8640 ev.

Figure 11: Unreliable ATIS reconstructions of an ArUco marker at 4 rps, sensitivity 20, strong lighting. Different number of events used for each reconstruction.

mean intensity of 2.6 ± 1.2.

With the Basler camera, ArUco marker detection works reliably up to 0.47 rps or 2.9 kpx/s image ve-

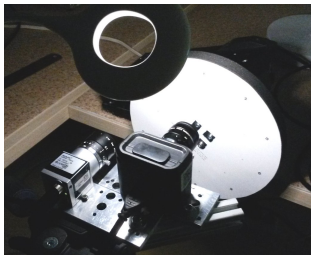

Figure 12: The experimental scene setup with weak lighting.

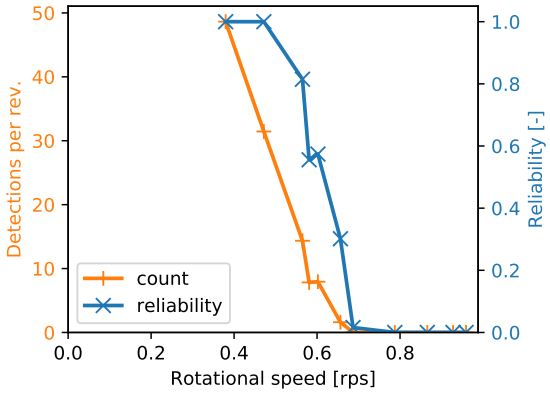

Figure 13: Reliability of marker detection with the Basler camera and mean count of single marker detections per revolution as functions of rotational speed. Weak lighting.

(a) 0.47 rps (b) 0.61 rps

Figure 14: Images of an ArUco marker captured by the Basler camera at weaker lighting. Exposure time 3000 μs. Different rotational speeds.

locity. 50% reliability is reached approximately for 0.61 rps or 3.7 kpx/s, see Figure 13. See Figure 14 for sample marker images at different angular speeds.

The signal-to-noise ratio of the ATIS event camera decreases with decreasing lighting intensity. To quantify this fact, we measured the ambient event rate generated by the event camera in a static scene, see Figure 15. In the case of sensitivity equal to 50, the noise event rate grows from 7000 events per second with strong lighting to 15000 events per second with weak lighting. This difference becomes even more pronounced with higher sensitivity settings.

The images reconstructed from the ATIS camera

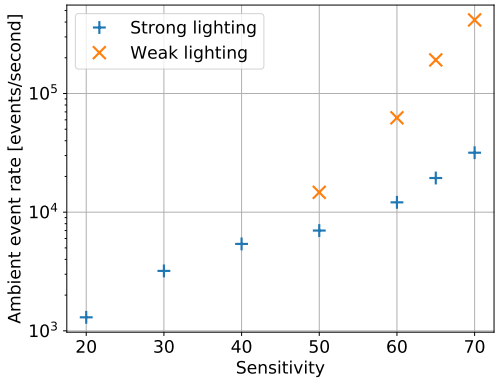

Figure 15: Maximum ambient (noise) event rate of the ATIS at the strong and weak lighting, as the function of contrast sensitivity. The event rate was measured on 10 ms long intervals.

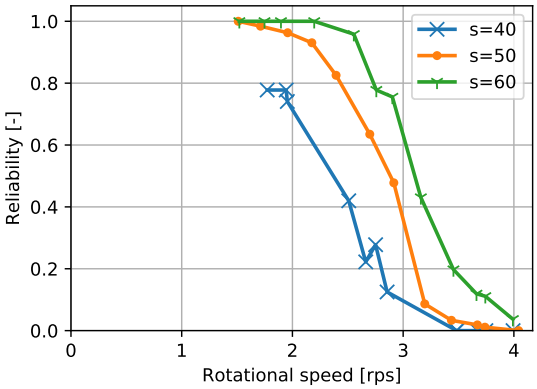

Figure 16: Reliability of marker detection using the ATIS as a function of rotational speed. For several sensitivity setting values s. Weak lighting.

events with the highest tested sensitivity setting of 60 enable reliable marker detection up to 2.2 rps or 13 kpx/s image velocity, see Figure 16. 3.1 rps or 19 kpx/s yield 50% reliability with the best performing sensitivity setting of 60. Lower sensitivities of 50 and 40 perform worse than 60. This time, unlike with the strong lighting, the same observation applies even to the detection count visualised in Figure 17. See Figure 18 for sample reconstructed marker images at different angular speeds and with different sensitivity settings.

5.3. Balistic experiment

To further test the ability of the ATIS sensor to read events from its pixel matrix, we recorded a 9 mm projectile freely flying at the speed of 300 m/s. The image velocity of the projectile was 220 kpx/s in

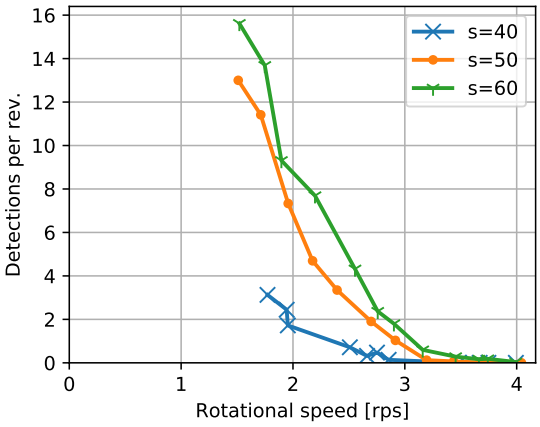

Figure 17: Mean count of single marker detections per revolution with the ATIS as a function of rotational speed. For several sensitivity setting values s. Weak lighting.

(a) 2.0 rps, $s = 40$ (b) 2.0 rps, $s = 60$ (c) 3.2 rps, $s = 60$

Figure 18: ATIS reconstructions of an ArUco marker from 8640 events per frame at weaker lighting. Different rotational speeds and sensitivities s.

ATIS, 620 kpx/s in Balser, 930 kpx/s in the Photron camera. ATIS sensitivity was set to 50. The resulting samples of event batches 20 μs long are in Figure 19, together with photos of the projectile taken by the Basler and the Photron cameras. The ATIS event rate did not exceed 6 million events per second. The projectile image from the Basler camera is significantly blurred, while the Photron image clearly shows the projectile shape.

When the projectile translated horizontally along the pixel rows of the ATIS, the sensor managed to read events from the entire projectile area in time. We also recorded the same flying projectile with the ATIS camera rotated by ninety degrees around the optical axis, to emulate vertical projectile translation. The visualisation of the vertical translation in Figure 19 suggests events omitted on entire pixel rows, resembling the results in Figure 9.

With the projectile moving mostly along the pixel rows, we are able to estimate the trajectory of the projectile directly from the ATIS events using a simple method. We process events in 10 μs long batches

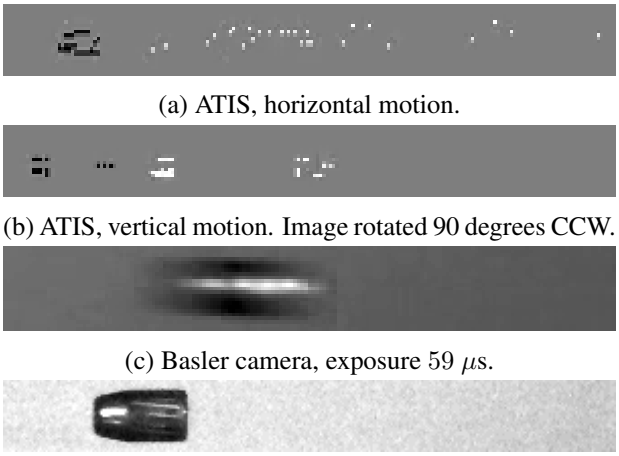

(a) ATIS, horizontal motion.

(b) ATIS, vertical motion. Image rotated 90 degrees CCW.

(c) Basler camera, exposure 59 μs.

(d) Photron camera., exposure 1 μs.

Figure 19: A 9 mm projectile freely flying at 300 m/s. 20 μs of recorded ATIS events and photos of the same scene from the Basler and Photron cameras.

and compute a bounding box of all negative polarity events within a batch. In the case of the Photron images, we threshold each image and compute the bounding box of its dark pixels. The centroid of a bounding box becomes the estimated projectile position.

Figure 20 shows the estimated projectile trajectories. The estimates from the Photron camera are more precise than from the ATIS thanks to its higher sensor resolution. The ATIS provided estimates at the rate of 100 kHz and the Photron at 20 kHz. We note, however, that the Photron rate can be increased to 100 kHz for image resolutions comparable to the resolution of the ATIS. The image velocities observed by the two cameras do not have the same direction because their optical axes were not aligned. The results from the Basler camera are not included in the plots as its low 1000 Hz frame rate would fail to capture the image of the projectile more than twice per run, even if the image velocity was only 220 kpx/s.

6. Discussion

With strong lighting, the ATIS event camera enables ArUco marker detection and classification at approx. 6$\times$ lower image velocity than the fast global shutter Basler camera. This limit is likely caused by the limited capacity of the event readout circuitry of the ATIS. As the image velocity increases, the circuitry more likely tends to ommit reading events generated by pixels in a subset of pixel rows during

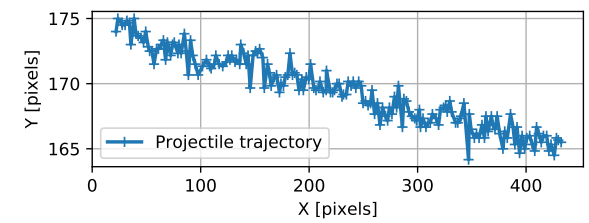

(a) ATIS camera.

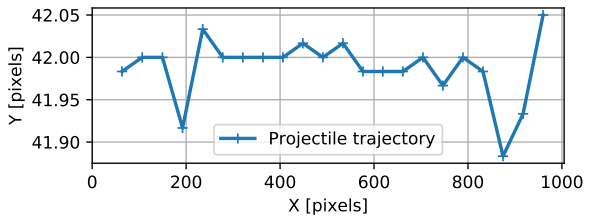

(b) Photron camera.

Figure 20: Sample image trajectory of a freely flying 9 mm projectile estimated from ATIS events and Photron camera images.

a 100 μs long interval. This readout jitter corrupts event timestamps and makes intensity image reconstruction more challenging.

Our experiment with the freely flying projectile suggests that the readout circuitry limits are more strict when most events come from a small number of columns, rather than from rows. Omissions of event data appear already at event rates below 6 million events per second. Furthermore, we believe that the estimated global event rate limit of 22 million events per second was not exceeded in any of our experiments.

The Basler camera is only limited by the motion blur when the scene lighting is strong. Weaker scene lighting demands larger exposure time which reduces the maximum motion speed with reliable marker detection.

Our experimental results suggest that the ATIS camera can detect markers moving $4.5\times$ faster than the Basler camera with weaker lighting. We note, however, that this difference may not be entirely caused by the event-based nature of the ATIS camera, as the pixel photodiode area of the ATIS sensor is at least two times larger than the same area in the Basler camera.

The ATIS performance drop due to weaker lighting is likely caused by a larger share of noise events, i.e. a lower signal to noise ratio. Noise events are caused by light shot noise. Shot noise more likely causes a sufficiently large apparent change in relative contrast when the light intensity is lower. Marker reconstruction from events works best with the highest tested ATIS sensitivity setting. This suggests that the amount of informative events gained from increased sensitivity outweighs the increased number of events triggered by shot noise.

The trailing events of positive polarity in Figure 19 are a mystery to us. They suggest that there may be an asymmetry in the pixel response latency to positive and negative high-speed contrast changes. Furthermore, the nature of the latency to positive changes would be stochastic. We asked the ATIS camera manufacturer Prophesee about this and about the event readout ommissions in December 2019 but did not receive an answer to the question before the 22nd of January 2020.

7. Conclusions

We constrained the scope of this work to understanding the limits of event cameras when sensing fast movement. Our experimental event camera data were generated by a single ATIS sensor.

A strongly lit square textured object of size 34×34 pixels with appearance similar to ArUco markers can be reliably recognised in images reconstructed from ATIS events when the object moves at most at 24 kpx/s image velocity. A global shutter camera with exposure time 59 μs can recognise the same object moving at $6\times$ higher image velocity. We believe the ATIS is limited by its event readout circuitry in this case. However, we think that this issue may be mitigated in future generations of event cameras.

When a dynamic scene generates the majority of events in a small number of pixel rows (e.g. seven), the event readout is more reliable. As a result, the position of a tiny object as fast as 220 kpx/s can be tracked at 100 kHz sampling rate by the ATIS.

The decrease in ATIS detection performance from 24 kpx/s to 13 kpx/s due to weaker lighting was likely caused by the decreased signal-to-noise ratio. Photon shot noise triggers relative contrast change events more likely when the light intensity is lower.

With the exception of tracking the position of a tiny object translating almost horizontally, we conclude that we have not found an application where the event camera is significantly better than the ordinary frame-based camera.

Acknowledgements

This work was supported by the European Regional Development Fund under project Robotics for Industry 4.0 (reg. no. $CZ.02.1.01/0.0/0.0/15\_003/0000470$).

We thank Libor Wagner for manufacturing and mounting the plastic disk for the experiment with rotating ArUco markers.

References

[1] P. Lichtsteiner, C. Posch, and T. Delbruck, "A 128 X 128 120dB 30mW Asynchronous Vision Sensor that Responds to Relative Intensity Change," in *2006 IEEE International Solid State Circuits Conference - Digest of Technical Papers*. IEEE, 2006. 1, 3

[2] G. Gallego, T. Delbrück, G. Orchard, C. Bartolozzi, B. Taba, A. Censi, S. Leutenegger, A. J. Davison, J. Conradt, K. Daniilidis, and D. Scaramuzza, "Event-based vision: A survey," *CoRR*, vol. abs/1904.08405, 2019. 2

[3] D. Scaramuzza, G. Gallego, and K. Daniilidis. (2019) Second International Workshop on Event-based Vision and Smart Cameras. [Online]. Available: http://rpg.ifi.uzh.ch/CVPR19_event_vision_workshop.html 2

[4] H. Rebecq, R. Ranftl, V. Koltun, and D. Scaramuzza, "Events-to-Video: Bringing Modern Computer Vision to Event Cameras," *IEEE Conf. Comput. Vis. Pattern Recog. (CVPR)*, 2019. 2, 3

[5] D. Falanga, S. Kim, and D. Scaramuzza, "How Fast Is Too Fast? The Role of Perception Latency in High-Speed Sense and Avoid," *IEEE Robotics and Automation Letters*, vol. 4, no. 2, pp. 1884–1891, 2019. 2

[6] J. Barrios-Avilés, T. Iakymchuk, J. Samaniego, L. Medus, and A. Rosado-Muñoz, "Movement Detection with Event-Based Cameras: Comparison with Frame-Based Cameras in Robot Object Tracking Using Powerlink Communication," *Electronics*, vol. 7, no. 11, p. 304, nov 2018. 2

[7] S. Garrido-Jurado, R. Muoz-Salinas, F. Madrid-Cuevas, and M. Marn-Jimnez, "Automatic Generation and Detection of Highly Reliable Fiducial Markers under Occlusion," *Pattern Recognition*, vol. 47, no. 6, pp. 2280 – 2292, 2014. 2

[8] H. Rebecq, R. Ranftl, V. Koltun, and D. Scaramuzza, "High Speed and High Dynamic Range Video with an Event Camera," *arXiv e-prints*, 2019. 2

[9] C. Posch, D. Matolin, and R. Wohlgenannt, "A QVGA 143 dB Dynamic Range Frame-free PWM Image Sensor with Lossless Pixel-level Video Compression and Time-Domain CDS," *IEEE Journal of Solid-State Circuits*, vol. 46, no. 1, pp. 259–275, Jan. 2011. 3

[10] C. Brandli, R. Berner, M. Yang, S.-C. Liu, and T. Delbruck, "A 240 X 180 130 dB 3 μs Latency Global Shutter Spatiotemporal Vision Sensor," *IEEE Journal of Solid-State Circuits*, vol. 49, no. 10, pp. 2333–2341, oct 2014. 3